







DOI: <http://dx.doi.org/10.1590/1807-1929/agriambi.v26n12p907-914>

## Estimating soil loss by laminar erosion using precision agriculture computational tools<sup>1</sup>

Estimativa da perda de solo por erosão laminar  
usando ferramentas computacionais na agricultura de precisão

Evelin T. S. Krug<sup>2</sup>, Glaucio J. Gomes<sup>2</sup>, Eduardo G. de Souza<sup>3</sup>,  
Luciano Gebler<sup>4</sup>, Ricardo Sobjak<sup>2</sup> & Claudio L. Bazzi<sup>2\*</sup>

<sup>1</sup> Research developed at Céu Azul, PR, and Serranópolis do Iguaçu, PR, Brazil

<sup>2</sup> Universidade Tecnológica Federal do Paraná/Programa de Mestrado em Tecnologias Computacionais para o Agronegócio, Medianeira, PR, Brazil

<sup>3</sup> Universidade Estadual do Oeste do Paraná/Programa de Engenharia Agrônômica, Cascavel, PR, Brazil

<sup>4</sup> Embrapa Uva e Vinho, Vacaria, RS, Brazil

### HIGHLIGHTS:

*The greater the stability of the aggregates in water, the lower the surface runoff.*

*The USLE makes it possible to identify places susceptible to erosion.*

*Computational tools optimize environmental conservation techniques.*

**ABSTRACT:** The study aimed to identify and evaluate the spatial variability in laminar erosion in areas using precision agriculture tools. Soil data from three properties in the western region of Paraná state, Brazil, were used: one in the municipality of Céu Azul (area A) and two in Serranópolis do Iguaçu (areas B and C). To identify discrepant data (outliers), analysis of the dispersion of quartiles was performed using a box-plot graph. Data normality was verified using the Kolmogorov-Smirnov test. A spatial analysis was performed using AgDataBox-Map software. The parameters of the universal soil loss equation were estimated and used with map algebra to produce a model to identify areas susceptible to erosion. Area A (soil loss estimate = 0-200 t ha<sup>-1</sup> per year) presented greater susceptibility to erosion than areas B and C (soil loss estimate = 0-150 t ha<sup>-1</sup> per year); however, all areas had a low susceptibility to erosion.

**Key words:** precision agriculture, thematic maps, geostatistics, universal soil loss equation, kriging

**RESUMO:** Esse estudo teve como objetivo avaliar e identificar a variabilidade espacial da erosão laminar em áreas que utilizam agricultura de precisão. Para tanto, foram utilizados dados de solo de três propriedades da região oeste do Paraná, uma no município de Céu Azul (área A) e duas em Serranópolis do Iguaçu (áreas B e C). Para identificar os dados discrepantes (outliers), foi realizada uma análise da dispersão dos quartis por meio de um gráfico box-plot. A verificação da normalidade dos dados foi realizada com base na aplicação do teste de Kolmogorov-Smirnov. Em seguida, foi realizada uma análise espacial, utilizando o software AgDataBox-Map. Após a obtenção dos mapas temáticos, foram estimados os parâmetros da Equação Universal de Perdas de Solo. Após essa etapa, foram calculados os fatores de estimativa das perdas de solo e gerados mapas temáticos, os quais foram integrados por álgebra cartográfica, resultando no modelo de identificação de áreas suscetíveis à erosão. A área A apresentou maior suscetibilidade (estimativa de perda de solo = 0-200 t ha<sup>-1</sup> por ano) quando comparada às áreas B e C (estimativa de perda de solo = 0-150 t ha<sup>-1</sup> por ano), porém, todas as áreas apresentam baixa suscetibilidade à erosão.

**Palavras-chave:** agricultura de precisão, mapas temáticos, geoestatística, equação universal de perda de solo, kriging



## INTRODUCTION

For the most part, soil degradation in agricultural areas is associated with water erosion and, consequently, low productivity (Li et al., 2022). Soil loss through crop harvesting also plays an important role and is often neglected. This phenomenon is very complex because it involves the direct and indirect action of several factors, such as geologic-geomorphological characteristics, soil types, climate, vegetation, and anthropic actions.

To estimate the annual rate of soil loss, a study assessed the erosion risk and mapped priority areas for soil and water conservation measures in Ethiopia using the revised universal soil loss equation (RUSLE) model developed in ArcGIS software (Woldemariam et al., 2018). The model of Woldemariam et al. (2018) provides a quantitative estimate of the rates of water-induced soil loss and the spatial distribution of erosion risk. In this context, many studies in Brazil have obtained satisfactory results in verifying different soil losses as a function of precipitation data using the universal soil loss equation (USLE) method (Mello et al., 2015; Didoné et al., 2021; Godoi et al., 2021; Silva et al., 2021). The USLE has been used in several studies (Bezak et al., 2021) and requires a relatively small amount of information when compared to more complex models. It is considered a good tool for predicting soil losses (Alewell et al., 2019) but has some limitations, considering that surface runoff is neglected in these models.

To understand the cause and effect of different erosive processes, geostatistical methods offer new technological concepts within soil-landscape relationships that may be key factors in forecasting models. The current study aimed to estimate soil loss by laminar erosion through quantitative prediction models in the agricultural areas of western Paraná state, Brazil, and to evaluate the impact of spatial variability using computational tools and equipment in the context of precision agriculture.

## MATERIAL AND METHODS

The study was conducted in three agricultural areas located in the western region of the state of Paraná, Brazil (Figure 1). Field A was located in the municipality of Céu Azul, with an average altitude of 653 m, an average slope of 4°, and a 15.5 ha area. Fields B (average altitude of 366 m and slope 2°) and C (average altitude of 301 m and slope 3°) were located in the municipality of Serranópolis do Iguaçu, with areas of 9.9 and 23.8 ha, respectively.

The soils in these fields were classified according to the methodology presented in a previous study (Gavioli et al., 2019). These soils were identified as typical oxisols and had been cultivated in a no-tillage system for at least 14 years, with a crop sequence of soybean, wheat, corn, and oat in field A, and with the succession of corn and soybean crops under a no-tillage system for at least 10 years in fields B and C.

The data used for this study were obtained from the Laboratory of Mechanization and Precision Agriculture (LAMAP) at UNIOESTE, Cascavel campus, in collaboration with the Federal Technological University of Paraná, Medianeira campus, which performed the sampling using irregular grids at 40 points in area A, 42 in area B, and 73 in area C (Figure 1). Around each point defined in the sampling grid, eight perforations (subsamples) were performed, two per quadrant, within a radius of 3 m from the central point at a depth of 0-0.2 m. The samples were homogenized, and a portion was removed to determine the soil particle size (clay, silt, and sand), pH, and organic matter (OM).

The variability in soil attributes was evaluated using exploratory data analysis. To identify discrepant data (outliers), analysis of the dispersion of quartiles was performed using a box-plot graph. Data normality was verified using the Kolmogorov-Smirnov test. Next, a spatial analysis was performed using AgDataBox-Map software to obtain the spatial variability of each variable. After data entry, the interpolation selection index was used to define the best interpolator.

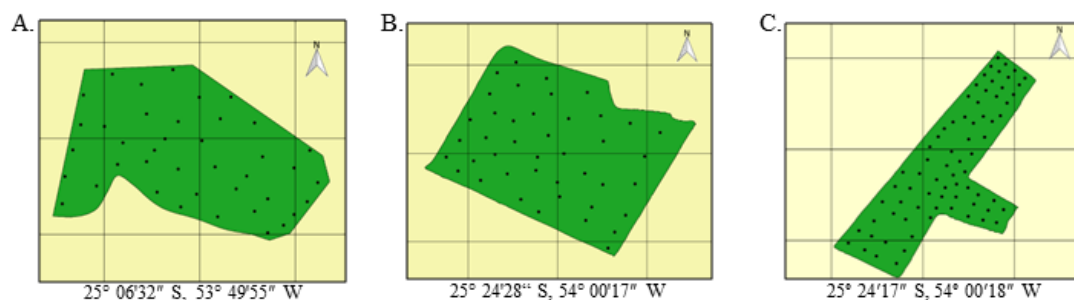
The best method was determined according to the value of the interpolation selection index (ISI), from which values for non-sampled locations were estimated, and maps of the spatial distribution of each variable were constructed. After obtaining thematic maps, the parameters of the universal soil loss equation (USLE) (Wischmeier & Smith, 1978), were calculated, where the estimated soil loss (A) was calculated according to Eq. 1.

$$A = R \cdot K \cdot LS \cdot C \cdot P \quad (1)$$

where:

- A - soil loss (t ha<sup>-1</sup> per year);
- R - rainfall erosivity (MJ mm ha<sup>-1</sup> h per year);
- K - soil erodibility factor (t ha h<sup>-1</sup> ha<sup>-1</sup> MJ<sup>-1</sup> mm<sup>-1</sup>);
- LS - slope length-gradient factor (dimensionless);
- C - land use and coverage factor (dimensionless); and,
- P - conservation practice factor (dimensionless).

Rainfall data from the hydrological information system of the instituto de águas do Paraná for the period 1997-2018,



Field A - Municipality of Céu Azul; Fields B and C - Municipality of Serranópolis do Iguaçu

**Figure 1.** Location of sampling points and contour of areas of the study sites. (A) Field A; (B) Field B; (C) Field C

comprising a series of 22 years for the cities of Céu Azul and Serranópolis do Iguaçu, were used to calculate the rainfall erosivity factor (R) (Eq. 2).

$$EI = 67.355 \left( \frac{r^2}{P} \right)^{0.85} \quad (2)$$

where:

- EI - monthly average erosivity index (MJ mm ha<sup>-1</sup> h<sup>-1</sup> per month);
- r - average monthly rainfall (mm); and,
- P - mean annual precipitation (mm).

Using the monthly average erosivity indices (EI), it was possible to calculate the annual R (Eq. 3).

$$R = \sum_{I=1}^{12} EI \quad (3)$$

where:

- R - annual erosivity (MJ mm ha<sup>-1</sup> h<sup>-1</sup> per year); and,
- EI - monthly average erosivity index (MJ mm ha<sup>-1</sup> h<sup>-1</sup> per month).

For erodibility (K factor), thematic maps of sand, silt, and clay generated in the AgDataBox-Map software were used. The K factor was calculated using the percentages of sand, silt, and clay in each sample by applying Eq. 4. From the results obtained, soil erodibility maps were generated for the three study areas.

$$K = \frac{(\%sand + \%silt)}{(\%clay)} / 100 \quad (4)$$

where:

- %sand - sand fraction;
- %silt - silt fraction; and,
- %clay - clay fraction of the soil under study.

The LS factor was obtained using radar image data from the Shuttle Radar Topography Mission (SRTM), code letter 025S54, provided by the geomorphometric database of Brazil, project topodata, with a spatial resolution of 30 m.

The SRTM image was cut using the contour of the study areas as a mask, the slope maps (S) were created using the minimum detectable effect (MDE) analysis tool, and the slope length (L) was calculated using the slope length function available in the SAGA GIS software (Conrad et al., 2015). After this step, the ramp length and slope data were multiplied by the raster calculator using Eq. 5.

$$LS = 0.00984\lambda^{0.63}D^{1.18} \quad (5)$$

where:

- LS - topographical factor;
- $\lambda$  - represents the length of the ramp, and,
- D - the slope of the land (%).

To calculate the use and management factor (C), vegetation cover in the study areas was assessed by calculating the normalized difference vegetation index (NDVI), which is a sensitive indicator of the quantity and condition of vegetation (Li et al., 2021). For image collection, the UAV Phantom 4 Advanced drone, equipped with a global positioning system/GLONASS, 20-megapixel camera with a 1-inch sensor, and a mechanical shutter was used. Another camera, Parrot Sequoia, was attached to the drone to collect infrared images. The flight plan was created using a drone-deployment tool (Drone Deploy).

The images were processed using Pix4D Mapper software, and a mosaic of images was generated for each area. The total coverage of each experimental area was then determined. After this step, the NDVI was calculated (Eq. 6).

$$NDVI = \frac{NIR - R}{NIR + R} \quad (6)$$

where:

- NDVI - Normalized Difference Vegetation Index; and,
- NIR - near infrared reflectance and R is red reflectance.

NDVI values ranged from -1 (lowest amount of vegetation) to 1 (highest amount of vegetation), and C values ranged from 0 (protected soil) to 1 (exposed soil). Considering this difference, the methodology proposed by Karaburun (2010) was used to correlate the two variables using linear regression. Finally, the P factor took the 0.5 value for the cultivation areas. After obtaining the thematic maps related to the parameters predicted by the USLE, they were combined to generate a single integrated map for each area, which was based on a set of operations performed for each pixel unit and facilitate the acquisition of a new layer of information corresponding to the erosion susceptibility map.

## RESULTS AND DISCUSSION

The data obtained through descriptive statistics (minimum, maximum, mean, median, standard deviation, coefficient of variation, skewness, and kurtosis) for the prior analysis of each field were subjected to dispersion analysis using boxplot representations. (Figure 2).

Outliers were identified for sand in Field A. For Field B, outliers were identified in the silt, clay, and pH datasets. In field C, outliers were identified in all variables, except for pH. After removing the outliers, all variables presented a normal distribution according to the Kolmogorov-Smirnov test. Soil from field A was sandier and had a higher pH than soil from fields B and C (Figure 2). This suggests that fields with a higher percentage of sand are less acidic, possibly because the presence of organic matter significantly affects the activity of soil microorganisms. Fields with higher clay content (fields B and C in Figure 2) had greater resistance to pH variation (higher buffering capacity) when compared to clayey areas (field A), due to the management of organic materials that influence the acidity of the soil.

Using AgDataBox-Map software, the interpolator and the respective parameters used in the interpolation process were

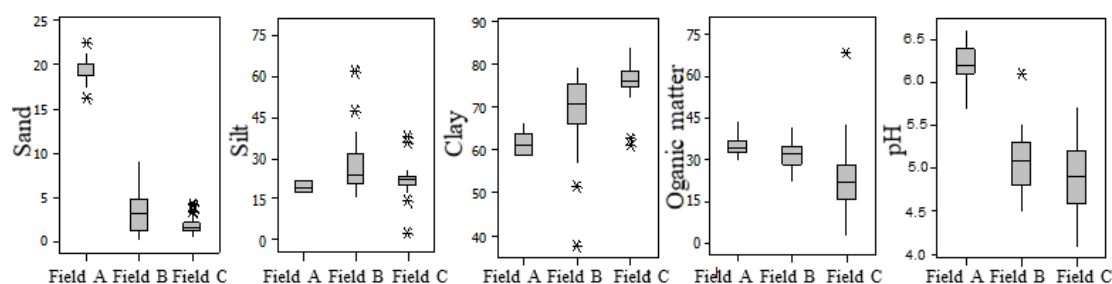


**Figure 2.** Boxplot Representations of the different soil properties determined in the areas investigated in Céu Azul (Field A) and Serranópolis do Iguaçú (Fields B and C)

defined using interpolation selection index (ISI) statistics. Only OM (Field B) and pH (Field C) were interpolated by Kriging, whereas for the other cases, the ISI statistics indicated better results by interpolation using inverse distance weighting (IDW) (Table 1).

Many studies suggest that Kriging presents better results (Shukla et al., 2020; Keshavarzi et al., 2021; Munyati & Sinthumule, 2021), however, in some cases, where the spatial dependence is considered weak, IDW is preferred. However, it is important to note that data variation is a dominant factor in method accuracy; as variation increases, method accuracy decreases (Li & Heap, 2011).

Figure 3 shows the thematic maps generated after interpolation of the variables. The maps of sand, silt, and clay have opposite distributions.

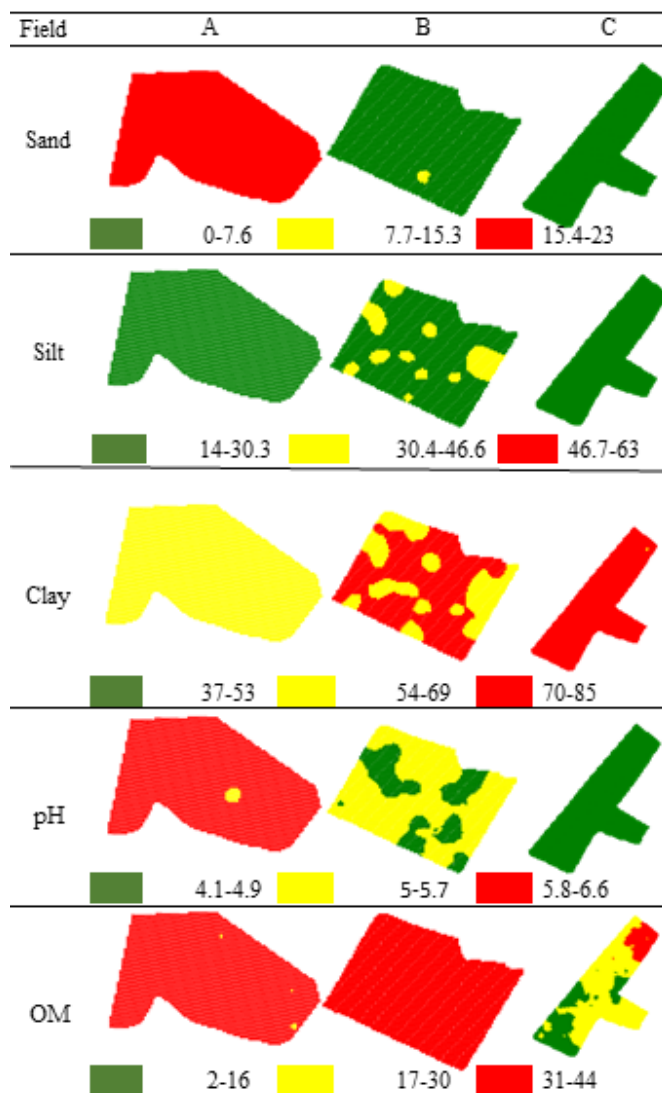
The soil fractions generally exhibit an inverse behavior, mainly in terms of distribution. Because they are measured as percentages, when there is a reduction in the one then there is an increase in the other. This concurs with the results of Souza et al. (2004), suggesting that the soil composition variables present a spatially dependent structure, with the greatest reach at depths of 0-0.2 m.

The organic matter content was higher in the lower part, coinciding with the lowest area of the land and greater sediment deposition. Gruba et al. (2015) demonstrated that the variation in the fine ( $\phi < 0.05$  mm) fraction (silt + clay) content had a major influence on the differences in the accumulation of soil organic carbon, particularly on its partitioning between the organic horizon and mineral soil. Other researchers (Angst et al., 2021) have demonstrated, through compiled data on microbial and plant-derived compounds in stabilized soil organic matter, that microbial compounds substantially contribute to stabilized soil organic matter. These authors identified that plant-derived compounds could account

**Table 1.** The best interpolation methods and parameters from AgDataBox-Map for each variable

Variable	ISI	Interpolator	Parameters
OM	0.055	OK	Mod: exponential, C0 = 20.2, C = 19.3, a = 119.6
pH	0.112	IDW	Exponential: 2, Nei: 5
Sand	0.048	IDW	Exponential: 1, Nei: 12
Silt	0.053	IDW	Exponential: 1, Nei: 9
Clay	0.107	IDW	Exponential: 1, Nei: 9
OM	0.247	IDW	Exponential: 1, Nei: 7
pH	0.050	OK	Mod: exponential, C0 = 0.11, C = 0.14, a = 262.0

OM - Organic matter; ISI - Interpolation selection index; IDW - Inverse distance weighting; OK - Ordinary Kriging; Nei - Number of neighbors; C0 - Nugget effect; C - Contribution effect; a - Tent



Field A - Municipality of Céu Azul; Fields B and C - Municipality of Serranópolis do Iguaçú; OM - Organic matter

**Figure 3.** Thematic maps of attributes of fields A, B, and C generated with five classes using the interpolation method

for ~50% of soil organic matter in aggregates and mineral-associated organic matter.

The parameters used to estimate soil loss were calculated using the erosivity factors of the cities of Céu Azul and Serranópolis do Iguaçú (Table 2).

In general, October has the highest precipitation, followed by January, May, November, and December (Table 2). The lowest average rainfall was recorded in July and August, consistent with the winter period. Similar results were reported for the state of São Paulo, where 60% of the intra-annual

**Table 2.** Mean monthly values of precipitation (mm) for the regions of Céu Azul and Serranópolis do Iguaçu

City*	JAN	FEB	MAR	APR	MAY	JUN	JUL	AUG	SEP	OCT	NOV	DEZ
CA	198.2	166	155.7	156	179.5	155.7	103.5	99.8	149.4	270.2	194.8	172.3
SI	193.8	158	157.3	145.6	179.9	152.1	107.4	97.5	144.2	245.2	167.6	166.3

\*CA - Céu Azul; SI - Serranópolis do Iguaçu

erosivity was concentrated between December and March; the highest values of erosivity due to rainfall are correlated with regions of greater agricultural activity (Teixeira et al., 2021). This is concerning, given that this period follows the harvest of winter crops and precedes the planting of summer crops leaves the soil unprotected and susceptible to erosion.

From the data in Table 2, the erosivity indices of the cities of Céu Azul and Serranópolis do Iguaçu were calculated (Table 3).

Extreme erosivities in Céu Azul were 12373.32 and 7606.54 MJ mm ha<sup>-1</sup> h<sup>-1</sup> per year in 2014 and 2001, respectively. For the municipality of Serranópolis do Iguaçu, the maximum erosivity was 11856.48 MJ mm ha<sup>-1</sup> h<sup>-1</sup> per year in 2014 and the minimum was 5851.70 MJ mm ha<sup>-1</sup> h<sup>-1</sup> per year in 2008.

The average annual erosivity (R) was obtained as 9267.74 MJ mm ha<sup>-1</sup> h<sup>-1</sup> per year for Céu Azul and 8791.63 MJ mm ha<sup>-1</sup> h<sup>-1</sup> per year for Serranópolis do Iguaçu. Waltrick et al. (2011) calculated the erosivity in 114 locations in Paraná state between 1986 and 2008, and included the municipality of Céu Azul, finding an average annual erosivity of 12121 MJ mm ha<sup>-1</sup> h<sup>-1</sup> per year, which is higher than the one calculated in the current study, while in the neighboring municipalities of Matelândia and São Miguel do Iguaçu, the values reported by Waltrick et al. (2011) were 11531 and 10701 MJ mm ha<sup>-1</sup> h<sup>-1</sup> per year, respectively.

The discrepancy in the values detected in this study and those reported by Waltrick et al. (2011) can be explained by the difference in the collection periods. The methodology does not consider the sediment deposition processes, and the

**Table 3.** Annual values of erosivity soil (MJ mm ha<sup>-1</sup> h<sup>-1</sup> per year) for the Municipalities of Céu Azul and Serranópolis do Iguaçu

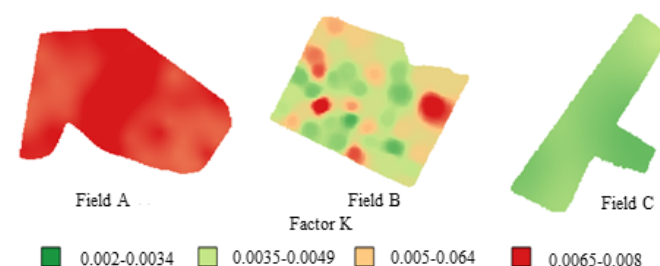
Year	Céu Azul	Serranópolis do Iguaçu
1997	9504.61	8962.55
1998	12086.92	10735.22
1999	8267.06	7562.03
2000	8283.65	7228.66
2001	7606.54	7743.26
2002	9805.35	9964.66
2003	8563.99	9395.14
2004	8345.88	8159.53
2005	9454.04	11286.24
2006	8944.01	6897.92
2007	8976.19	7501.21
2008	8866.72	5851.70
2009	10073.18	9434.14
2010	8383.66	8326.90
2011	10114.38	8057.30
2012	7617.77	7248.44
2013	10130.10	9759.34
2014	12373.32	11856.48
2015	10562.11	9344.72
2016	7961.93	8568.36
2017	10281.88	10300.09
2018	7687.01	9231.98
Mean	9267.74	8791.63

soil losses in rainy and dry periods are not weighted because the average rainfall is used in the equations. The erodibility factors were obtained using clay, site, and sand data presented in the thematic maps (Figure 3). The erodibility values and maps of the geocoded sampling points were interpolated in a geographic information system environment through Kriging (Figure 4).

To carry out a quantitative study of erosion in fields A, B, and C, the K factor was used, as it incorporates all the physical properties of the soil that are the main determinants of erodibility (Olaniya et al., 2020). In field A, the values ranged from 0.0057 to 0.0068 t ha h<sup>-1</sup> ha<sup>-1</sup> MJ<sup>-1</sup> mm<sup>-1</sup> with greater erodibility in the central part of the plot. In fields B and C, erodibility varied from 0,0024 to 0.0076 t ha h<sup>-1</sup> ha<sup>-1</sup> MJ<sup>-1</sup> mm<sup>-1</sup> and from 0.0026 to 0.0034 t ha h<sup>-1</sup> ha<sup>-1</sup> MJ<sup>-1</sup> mm<sup>-1</sup>, respectively, indicating that erodibility was lower than that in field A. In field A, higher values of K were determined because of the greater amount of sand and fine sand contents that do not have adhesion properties and are easily transported. Fields B and C had a more clayey texture that, when combined with the presence of organic matter and moisture, increased the stability of aggregates and sand fractions and reduces erodibility. These areas had very low erodibility values (R < 0.009), which is consistent with the soil in the region. Oxisols have characteristics such as advanced evolution, are very weathered, and are deep; therefore, they are less susceptible to erosion (Pasquatto & Tomazoni, 2016).

The highest clay values were concentrated in areas with lower erodibility. The structure of the soil influences its resistance to water erosion through the physicochemical properties of the clay, which contribute to the stability of the aggregates in the presence of water and biological factors. Thus, the greater the stability of the aggregates in water, the greater the permeability of the soil and the lesser the disaggregation, and consequently, the lower the surface runoff and the drag of particles by the water. K values in other studies for oxisols were 0.03, 0.041, and 0.01 t ha h<sup>-1</sup> ha<sup>-1</sup> MJ<sup>-1</sup> mm<sup>-1</sup>, and the calculated K value is lower than the values found in the literature (Demarchi & Zimback, 2014; Pasquatto & Tomazoni, 2016). This difference can be explained by the difference in the size of the study area and precision of the data used.

The topographic factor was calculated using the slope map (S) generated by MDE analysis, and the slope length (L)



Field A - Municipality of Céu Azul; Fields B and C - Municipality of Serranópolis do Iguaçu  
**Figure 4.** Erodibility of study areas (K, t ha h<sup>-1</sup> ha<sup>-1</sup> MJ<sup>-1</sup> mm<sup>-1</sup>)

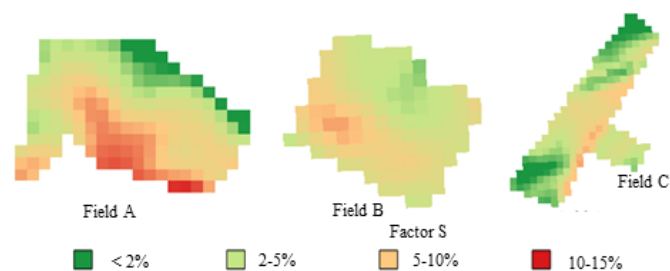
was calculated using the slope length function of SAGA GIS software. Figures 5 and 6 show the maps generated for fields A, B, and C.

The LS (length/slope) factor was calculated using a raster calculator after obtaining the slope and ramp length data. Figure 7 presents the results of the LS factor obtained for each field (A, B, and C).

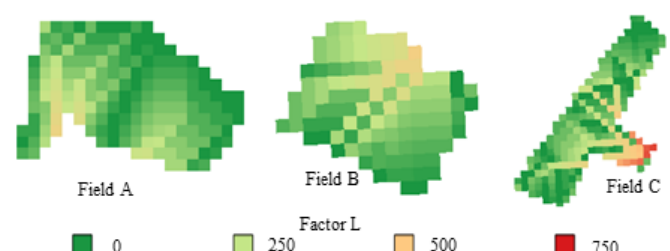
The volume and speed of the floods are directly related to the degree of slope of the terrain; thus, as observed, areas with greater slopes have a higher LS factor. Despite this, it is observed that there is a predominance of values between 0 and 4, with a greater representation of values close to zero, indicating that a large part of the study area had lower rates of runoff, which is not conducive to laminar water erosion.

According to Fornelos & Neves (2007), LS values between 0 and 1 are very low, those between 1 and 2 are low, and those between 2 and 5 are moderate. The land use and occupation factors (C) were obtained through the correlation of the values of NDVI and Factor C attributed by Pasquatto & Tomazoni (2016) (Figure 8). From this correlation, the land use and occupation factors (C) are shown in Figure 8.

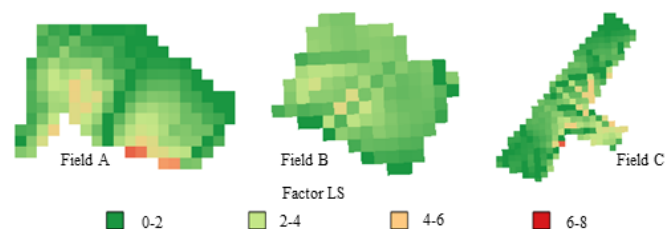
As noted, the highest values are associated with areas that have little or no ground cover, represented in red. The yellow color represents the presence of dead vegetation left over from direct planting. Factors C and P work separately



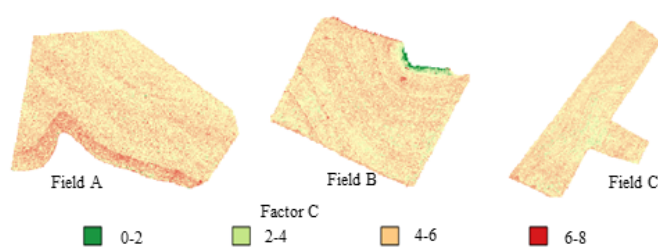
Field A - Municipality of Céu Azul; Fields B and C - Municipality of Serranópolis do Iguaçú  
**Figure 5.** Slope (S, %) of the study areas



Field A - Municipality of Céu Azul; Fields B and C - Municipality of Serranópolis do Iguaçú  
**Figure 6.** Slope length (L, m) of the study areas



Field A - Municipality of Céu Azul; Fields B and C - Municipality of Serranópolis do Iguaçú  
**Figure 7.** Topographic Factor (LS) of the study fields (length slope factor)



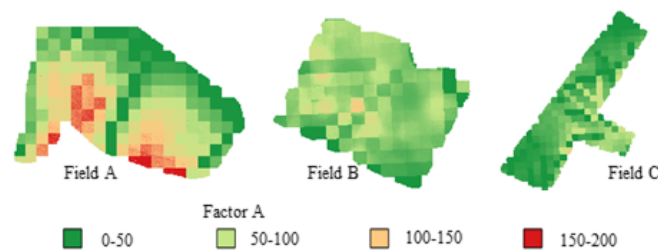
Field A - Municipality of Céu Azul; Fields B and C - Municipality of Serranópolis do Iguaçú  
**Figure 8.** Land use and occupation maps for the study areas

only when the objective is to define more adequate forms of agricultural production to reduce the impacts generated in the physical environment. Thus, the C factor map was multiplied by the Raster calculator by the P factor (0.5), as proposed by Fornelos & Neves (2007) for no-tillage soil. The model was used to calculate the average annual soil loss rates for fields A, B, and C, using thematic maps related to the parameters predicted by the USLE (Eq. 1) (Figure 9).

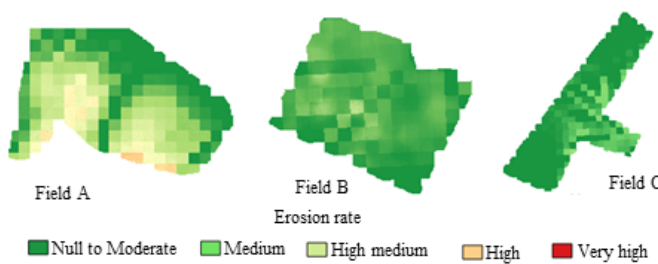
The estimated values of soil loss in field A varied from 0 to 192 t ha<sup>-1</sup> per year, while in fields B and C, soil loss rates ranged from 0 to 100 t ha<sup>-1</sup> per year, indicating a greater soil loss by erosion in field A. These results agree with the data presented in Figure 3. Analyzing the maps of the other factors in field A, it was observed that the highest values were found in the region with the highest slope; when compared to the LS factor, the maps were quite similar. In fields B and C, as expected, the estimated soil loss values were very close, differing mainly by the LS factor. The values estimated by the model shown in Figure 9 were evaluated using the erosion rate classification proposed by Cavallo (2008).

The susceptibility to erosion in the studied fields was mapped (Figure 10).

As described, field A was more susceptible to erosion than fields B and C; however, they all had low susceptibility to laminar erosion. Considering that the most influential



Field A - Municipality of Céu Azul; Fields B and C - Municipality of Serranópolis do Iguaçú  
**Figure 9.** The mean annual soil loss rates of fields A, B, and C (t ha<sup>-1</sup> per year)



Field A - Municipality of Céu Azul; Fields B and C - Municipality of Serranópolis do Iguaçú  
**Figure 10.** Maps of susceptibility to water erosion for fields A, B and C

factor is slope, it is important to use techniques that minimize runoff. Conservation practices depend on the location, the region's climate and soil characteristics, and the degree of soil degradation; however, common practices, such as correcting soil fertility and planting in contour lines in soils with slopes should be considered mandatory.

## CONCLUSIONS

1. The fields evaluated presented a low estimate of annual soil loss, with the area in the municipality of Céu Azul (field A) having the greatest spatial variability. Topography had the greatest influence, emphasizing the importance of adopting conservation techniques to minimize soil losses and reduce environmental impacts.

2. The tools used (as well as the methodology proposed) to assess the rates of soil loss due to laminar erosion increased the efficiency of the model's response, making it possible to estimate in greater detail the locations with greater susceptibility to erosion, facilitating guidance of appropriate management practices in the study regions.

## ACKNOWLEDGMENTS

The authors are grateful to the Universidade Estadual do Oeste do Paraná (UNIOESTE), the Universidade Tecnológica Federal do Paraná (UTFPR), the Fundação Araucária, the Coordenação de Aperfeiçoamento de Pessoal de Nível Superior (CAPES), the Conselho Nacional de Desenvolvimento Científico e Tecnológico (CNPq), and the Fundação Parque Tecnológico Itaipu (FPTI), for the support received.

## LITERATURE CITED

- Alewell, C.; Borrelli, P.; Meusburger, K.; Panagos, P. Using the USLE: Chances, challenges and limitations of soil erosion modelling. *International Soil and Water Conservation Research*, v.7, p.203-225, 2019. <https://doi.org/10.1016/j.iswcr.2019.05.004>
- Angst, G.; Mueller, K. E.; Nierop, K. G. J.; Simpson, M. J. Plant- or microbial-derived? A review on the molecular composition of stabilized soil organic matter. *Soil Biology and Biochemistry*, v.156, p.1-16, 2021. <https://doi.org/10.1016/j.soilbio.2021.108189>
- Bezak, N.; Mikoš, M.; Borrelli, P.; Alewell, C.; Alvarez, P.; Anache, J. A. A.; Baartman, J.; Ballabio C.; Biddoccu, M.; Cerdà, A.; Chalise, D.; Chen, S.; Chen, W.; De Girolamo, A. M.; Gessesse, G. D.; Deumlich, D.; Diodato, N.; Efthimiou, N.; Erpul, G.; Fiener, P.; Freppaz, ; Gentile, F.; Gericke, A.; Haregeweyn, N.; Hu, B.; Jeanneau, A.; Kaffas, K.; Kiani-Harchegani, M.; Villuendas, I. L.; Li, C.; Lombardo, L.; López-Vicente, M.; Lucas-Borja, M. E.; Maerker, M.; Miao, C.; Modugno, S.; Möller, M.; Naipal, V.; Nearing, M.; Owusu, S.; Panday, D.; Patault, E.; Patriche, C. V.; Poggio, L.; Portes, R.; Quijano, L.; Rahdari, M. R.; Renima, M.; Ricci, G. F.; Rodrigo-Comino, J.; Saia, S.; Samani, A. N.; Schillaci, C.; Syrris, V.; Kim, H. S.; Spinola, D. N.; Oliveira, P. T.; Teng, H.; Thapa, R.; Vantas, K.; Vieira, D.; Yang, J. E.; Yin, S.; Zema, D. A.; Zhao, G.; Panagos, P. Soil erosion modelling: A bibliometric analysis. *Environmental Research*, v.197, p.1-16, 2021. <https://doi.org/10.1016/j.envres.2021.111087>
- Carvalho, N. de O. *Hidrossedimentologia Prática*. 2.ed. Interciência, 2008. 600p.
- Conrad, O.; Bechtel, B.; Bock, M.; Dietrich, H.; Fischer, E.; Gerlitz, L.; Wehberg, J.; Wichmann, V.; Böhner, J. System for Automated Geoscientific Analyses (SAGA) v.2.1.4. *Geoscientific Model Development*, v.8, p.1991-2007, 2015. <https://doi.org/10.5194/gmd-8-1991-2015>
- Demarchi, J. C.; Zimback, C. R. L. Mapeamento, erodibilidade e tolerância de perda de solo na Sub-Bacia do Ribeirão das Perobas. *Energia na Agricultura*, v.29, p.102-114, 2014. <https://doi.org/10.17224/EnergAgric.2014v29n2p102-114>
- Didoné, E. J.; Minella, J. P. G.; Piccilli, D. G. A. How to model the effect of mechanical erosion control practices at a catchment scale?. *International Soil and Water Conservation Research*, v.9, p.370-380, 2021. <https://doi.org/10.1016/j.iswcr.2021.01.007>
- Fornelos, L. F.; S. M. A. S. Neves. Uso de modelos digitais de elevação (MDE) gerados a partir de imagens de radar interferométrico (SRTM) na estimativa de perdas de solo. *Revista Brasileira de Cartografia*, v.59, p.25-33, 2007.
- Gavioli, A.; Souza, E. G. de; Bazzi, C. L.; Schenatto, K.; Betzek, N. M. Identification of management zones in precision agriculture: An evaluation of alternative cluster analysis methods. *Biosystems Engineering*, v.81, p.86-102, 2019. <https://doi.org/10.1016/j.biosystemseng.2019.02.019>
- Godoi, R. de F.; Rodrigues, D. B. B.; Borrelli, P.; Oliveira, P. T. S. High-resolution soil erodibility map of Brazil. *Science of The Total Environment*, v.781, p.1-10, 2021. <https://doi.org/10.1016/j.scitotenv.2021.146673>
- Gruba, P.; Socha, J.; Błońska, E.; Lasota, J.; Effect of variable soil texture, metal saturation of soil organic matter (SOM) and tree species composition on spatial distribution of SOM in forest soils in Poland. *Science of The Total Environment*, v.521-522, p.90-100, 2015. <https://doi.org/10.1016/j.scitotenv.2015.03.100>
- Karaburun, A. Estimation of C factor for soil erosion modeling using NDVI in Buyukcekmece watershed. *Ozean Journal of Applied Sciences*, v.3, p.77-85, 2010.
- Keshavarzi, A.; Tuffour, H. O.; Brevik, E. C.; Ertunç, G. Spatial variability of soil mineral fractions and bulk density in Northern Ireland: Assessing the influence of topography using different interpolation methods and fractal analysis. *Catena*, v.207, p.1-17, 2021. <https://doi.org/10.1016/j.catena.2021.105646>
- Li, H.; Zhu, H.; Liang, C.; Wei, X.; Yao, Y. Soil erosion significantly decreases aggregate-associated OC and N in agricultural soils of Northeast China. *Agriculture, Ecosystems & Environment*, v.323, p.1-11, 2022. <https://doi.org/10.1016/j.agee.2021.107677>
- Li, J.; Heap, A. D. A review of comparative studies of spatial interpolation methods in environmental sciences: Performance and impact factors. *Ecological Informatics*, v.6, p.228-241, 2011. <https://doi.org/10.1016/j.ecoinf.2010.12.003>
- Li, S.; Xu, L.; Jing, Y.; Yin, H.; Li, X.; Guan, X. High-quality vegetation index product generation: A review of NDVI time series reconstruction techniques. *International Journal of Applied Earth Observation and Geoinformation*, v.105, p.1-18, 2021. <https://doi.org/10.1016/j.jag.2021.102640>
- Mello, C. R. de; Viola, M. R.; Owens, P. R.; Mello, J. M. de; Beskow, S. Interpolation methods for improving the RUSLE R-factor mapping in Brazil. *Journal of Soil and Water Conservation*, v.70, p.82-197, 2015. <https://doi.org/10.2489/jswc.70.3.182>

- Munyati, C.; Sinthumule, N. I. Comparative suitability of ordinary kriging and Inverse Distance Weighted interpolation for indicating intactness gradients on threatened savannah woodland and forest stands. *Environmental and Sustainability Indicators*, v.12, p.1-11, 2021. <https://doi.org/10.1016/j.indic.2021.100151>
- Olaniya, M.; Bora, P. K.; Das, S.; Chanu, P. H. Soil erodibility indices under different land uses in Ri-Bhoi district of Meghalaya (India). *Scientific Reports*, v.10, p.1-13, 2020. <https://doi.org/10.1038/s41598-020-72070-y>
- Pasquatto, M. C.; Tomazoni, J. C. Estudo do processo erosivo laminar na bacia de captação do rio Barro Preto, em Coronel Vivida - PR. *Revista Brasileira de Geografia Física*, v.9, p.555-570, 2016. <https://doi.org/10.26848/rbgf.v9.2.p555-570>
- Shukla, K.; Kumar, P.; Mann, G. S.; Khare, M. Mapping spatial distribution of particulate matter using Kriging and Inverse Distance Weighting at supersites of megacity Delhi. *Sustainable Cities and Society*, v.54, p.1-12, 2020. <https://doi.org/10.1016/j.scs.2019.101997>
- Silva, L. de C. M. da; Avanzi, J. C.; Peixoto, D. S.; Merlo, M. N.; Borghi, E.; Resende, A. V. de; Acuña-Guzman, S. F.; Silva, B. M. Ecological intensification of cropping systems enhances soil functions, mitigates soil erosion, and promotes crop resilience to dry spells in the Brazilian Cerrado. *International Soil and Water Conservation Research*, v.9, p.591-604, 2021. <https://doi.org/10.1016/j.iswcr.2021.06.006>
- Souza, Z. M.; Marques Júnior, J.; Pereira, G. T.; Barbieri, D. M. Spatial variability of the texture in an eutroxic red latosol under sugarcane crop. *Engenharia Agrícola*, v.24, p.1-11, 2004. <https://doi.org/10.1590/S0100-69162004000200009>
- Teixeira, D. B. de S.; Cecílio, R. A.; Oliveira, J. P. B. de; Almeida, L. T. de; Pires, G. F. Rainfall erosivity and erosivity density through rainfall synthetic series for São Paulo State, Brazil: Assessment, regionalization and modeling. *International Soil and Water Conservation Research*. Available on: <<https://www.sciencedirect.com/science/article/pii/S2095633921000952?via%3Dihub>>. Accessed on: Oct. 2021.
- Waltrick, P. C.; Machado, M. A. de M.; Oliveira, D. de; Grimm, A. M.; Dieckow, J. Erosividade de chuvas do Paraná: Atualização e influência dos eventos “El Niño” e “La Niña”. 1.ed. Sociedade Brasileira de Ciência do Solo: Núcleo Estadual do Paraná, 2011. 26p.
- Wischmeier, W. H.; Smith, D. D. Predicting rainfall erosion losses : a guide to conservation planning. USDA publications, 1978. 58p.
- Woldemariam, G. W.; Anteneh D. I.; Solomon T.; Ramireddy U. R. Spatial Modeling of Soil Erosion Risk and Its Implication for Conservation Planning: the Case of the Gobebe Watershed, East Hararghe Zone, Ethiopia. *Land*, v.7, p.1-25, 2018. <https://doi.org/10.3390/land7010025>